

Electric-Field-Controlled Cold Dipolar Collisions between Trapped CH₃F Molecules

M. Koller¹, F. Jung, J. Phrompao¹, M. Zeppenfeld¹, I. M. Rabey, and G. Rempe
 Max-Planck-Institut für Quantenoptik, Hans-Kopfermann-Strasse 1, 85748 Garching, Germany



(Received 1 February 2022; accepted 21 April 2022; published 17 May 2022)

Reaching high densities is a key step toward cold-collision experiments with polyatomic molecules. We use a cryofuge to load up to 2×10^7 CH₃F molecules into a boxlike electric trap, achieving densities up to $10^7/\text{cm}^3$ at temperatures around 350 mK where the elastic dipolar cross section exceeds $7 \times 10^{-12} \text{ cm}^2$. We measure inelastic rate constants below $4 \times 10^{-8} \text{ cm}^3/\text{s}$ and control these by tuning a homogeneous electric field that covers a large fraction of the trap volume. Comparison to *ab initio* calculations gives excellent agreement with dipolar relaxation. Our techniques and findings are generic and immediately relevant for other cold-molecule collision experiments.

DOI: [10.1103/PhysRevLett.128.203401](https://doi.org/10.1103/PhysRevLett.128.203401)

Polar molecules offer research opportunities that are not shared by other particles such as atoms [1]. The strong and long-range electric dipole-dipole interaction in particular can affect quantum-chemical reaction pathways [2–6], can induce large-scale correlations and novel phases in molecular quantum gases [7–11], and can be the basis for a robust quantum-computing architecture [12–17]. Toward these applications, closed-shell symmetric-top molecules stand out as an ideal platform due to their simple rotational energy-level structure, favorable matrix elements for cycling transitions [18], and linear response to an electric field [19]. Together, these properties have allowed for direct cooling and trapping of the numerically largest samples of ultracold molecules to date [20].

Further key requirements must be fulfilled to explore and leverage the dipole-dipole interaction between such molecules: first, observing dipolar collisions needs a high density combined with a long hold time. The latter can be accomplished by trapping the molecules [21–29]. Second, a high state purity is needed so that collision channels can be studied cleanly. This requires cooling the rotation of the molecules [30–32]. Also cooling the motion has the additional advantage that it increases the elastic cross section and decreases the number of inelastic collision channels [33]. Third, manipulating the collision process calls for a suitable control technique that must be compatible with the aforementioned cooling and trapping [34–37]. All demands have been met for ultracold dimers synthesized from laser-cooled [3,38–44] and directly cooled diatomic molecules

[45–47]. However, despite early attempts [48] and recent advances [49–51], collision studies with polyatomic molecules are still at a beginning.

Here we observe cold collisions between electrically trapped CH₃F molecules in a predominantly single rotational state. Moreover, we use a homogeneous electric field to tune the rate of inelastic two-body collisions. Excellent agreement between experimental data and a semiclassical model identifies the dominant loss mechanism to be dipolar relaxation [52] to untrapped rotational states. Understanding and controlling this mechanism is a *sine qua non* requirement for future thermalization and evaporative cooling experiments with molecules that can be decelerated, trapped and cooled, but are still far from the quantum regime.

The starting point for our collision measurements is to create a high-density sample of CH₃F molecules confined in an electric trap. As a molecule source we employ our Cryofuge [49], illustrated in Fig. 1(a), which combines cryogenic buffer-gas cooling [53] with centrifuge deceleration [54] to produce a continuous, high-flux beam of trappable ($\leq 25 \text{ m/s}$) molecules. The beam is velocity filtered by a sharply bent electric quadrupole [55] *s* piece that connects the exit of the centrifuge with the input of the trap. This prevents the fast velocity tail of the guided molecules from reaching the trap. Loading is turned on and off by simultaneously switching the guide connecting the cryogenic cell to the centrifuge decelerator and the *s* piece between guiding and nonguiding configuration [55]. We tune the trap loading rate by varying the electric field of the connection guide between 2 kV/cm for low flux and 20 kV/cm for high flux ($\sim 10^8/\text{s}$).

Our trap employs an electric multipole configuration that confines cold molecules in a boxlike potential [26]. It consists of a pair of microstructured capacitor plates, separated by 3 mm, and a surrounding ring electrode. Alternating voltages $\pm V_{\text{trap}}$ are applied to the microstructure

Published by the American Physical Society under the terms of the [Creative Commons Attribution 4.0 International license](https://creativecommons.org/licenses/by/4.0/). Further distribution of this work must maintain attribution to the author(s) and the published article's title, journal citation, and DOI. Open access publication funded by the Max Planck Society.

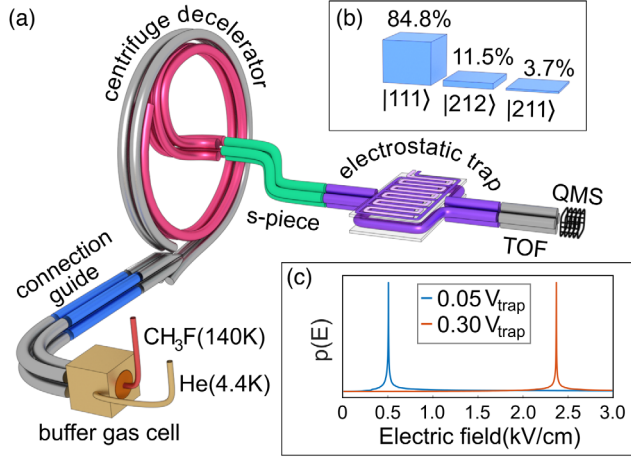


FIG. 1. Experimental setup. (a) CH_3F are cooled in a cryogenic buffer-gas cell (helium at 4.4 K) and transferred to a centrifuge decelerator by an electric connection guide. An s -shaped guide acts as a velocity filter connecting the exit of the centrifuge to the inlet of the electric trap. A mass spectrometer at the end of a time-of-flight guide attached to the trap outlet detects the molecules. (b) Measured state distribution in the trap, given in the symmetric-top basis $|J, K, M\rangle$. (c) Simulated electric-field distribution [20] of the electrostatic trap for $E_c = 0.50$ kV/cm (blue) and $E_c = 2.37$ kV/cm (red). The field is homogeneous ($\leq 10\%$ relative deviation from E_c) over $\sim 50\%$ of the geometric trap volume.

electrodes to provide strong confinement in the vertical direction, while the ring electrode with voltage V_{ring} provides confinement in the other two horizontal dimensions. For all measurements presented here, the trapping and ring electrode voltages are fixed to $V_{\text{trap}} = 1200$ V and $V_{\text{ring}} = 3V_{\text{trap}}$, resulting in a maximum trapping field of $E_{\text{trap}} = 40$ kV/cm. This confines molecules up to kinetic energies corresponding to ~ 1 K. A voltage difference applied to the capacitor plates creates a homogeneous electric control field E_c that covers $\sim 50\%$ of the trapped molecule ensemble and is tuned between 0.50 and 2.37 kV/cm, see Fig. 1(c).

Molecules are unloaded from the trap via a time-of-flight quadrupole guide, depicted in Fig. 1(a), that can be toggled on and off to measure the velocity distribution of the trapped sample (see Supplemental Material [56]). A quadrupole mass spectrometer (QMS) at the end of the guide detects the unloaded molecules, with the integrated signal being proportional to the density of trapped molecules n . Its time evolution can be modeled by

$$\frac{d}{dt}n(t) = \lambda(t) - \Gamma n(t) - kn^2(t), \quad (1)$$

with λ denoting the loading rate of molecules into the trap. Single-body loss from collisions with residual background gas, Majorana transitions for molecules passing through electric-field minima [62,63], or molecules leaving the trap

through the input and output guides [26,63] are characterized by a single-body loss rate Γ . The density-dependent collision-induced trap losses are given by the two-body loss-rate coefficient k .

The standard approach to measure two-body loss is to observe a density-dependent nonexponential decay of the trapped sample, clearly distinct from a single-body exponential decay [45]. We know, however, that in our trap Γ depends strongly on the molecule velocity v (proportional to v^5 for a linear Stark shift [63]). This causes deviations from a single-exponential decay even in the absence of collisions, i.e., in the limit of small density. However, for hold times less than 1 s, single-body loss can be approximated by a single-exponential decay (see Supplemental Material [56]). A further problematic effect arises when tuning the loading rate. Despite all precautions, changing the connection guide voltage creates small changes in the velocity distribution of the trapped samples, affecting the single-body decay rate by an amount similar to that due to collisions. To counter these complications, we developed a new measurement scheme that is robust against small changes of Γ (see Supplemental Material [56]), allowing us to extract a precise value for k as described in the following.

Our measurement scheme combines the results of three distinct experiments with three molecular samples A , B , and $A + B$, with the trap effectively serving as a test tube. The two samples A and B are created independently and are separated by their loading times, as illustrated in Figs. 2(a) and 2(b),

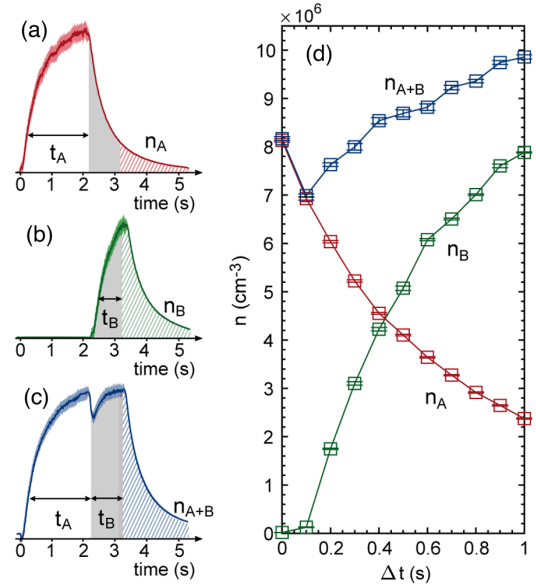


FIG. 2. Molecule signals. (a)–(c) Measurement sequences for samples A , B , and $A + B$. The gray areas depict the interaction time Δt , whereas the dashed areas illustrate the trap unloading signals which, when integrated, are proportional to the density of trapped molecules. (d) Density of trapped molecules as a function of the interaction time Δt for the A , B , and $A + B$ samples, recorded at $E_c = 0.50$ kV/cm.

respectively. Sample *A* is created by loading the trap for two seconds, reaching a steady state. At this time we stop the loading, wait 100 ms for transient effects to disappear, and start the interaction period, $\Delta t \in [0, 1]$ s [gray-shaded area in Figs. 2(a)–2(c)], during which collisions occur. The density n_A then evolves according to Eq. (1) with $\lambda_A = 0$. Similarly, we create sample *B* by turning on the loading rate λ_B for up to one second. We consider this to happen during the interaction period, but in the absence of sample *A*. For both samples, *A* and *B*, molecules are lost due to trap and collision losses between molecules, *A-A* collisions in sample *A* and *B-B* collisions in sample *B*. Finally, we create the third combined sample *A + B* by consecutively loading first sample *A* and then sample *B*, as illustrated in Fig. 2(c). This allows for additional loss only by means of *A-B* collisions during the interaction period Δt , as both individual samples are independent in all other respects. Figure 2(d) shows the integrated trap unloading signals for the *A*, *B*, and *A + B* samples as a function of Δt . We then combine the densities measured in the three samples, $\delta n(t) = n_A(t) + n_B(t) - n_{A+B}(t)$, to extract the (positive) collision signal δn .

Experimentally, we tune the density of trapped CH_3F molecules by changing the electric field in the connection guide and record δn as a function of \bar{n}^2 , defined as the product of $n_A(t)$ and $n_B(t)$ averaged over Δt . Results for $\Delta t = 1$ s are displayed in Fig. 3(a) for $E_c = 0.50$ kV/cm and $E_c = 2.37$ kV/cm. The observed linear dependence of δn on \bar{n}^2 proves, first, the existence of collisions (average collision energy $\sim k_B \times 0.4$ K) and, second, their nature as two-body loss process. The third observation refers to the clearly distinct slopes for the two control fields. This points to an electric-field dependence of k that we investigate in the following.

To extract a precise value for k we derive an expression for the time evolution of the collision signal δn during the interaction period Δt , and fit this expression to the measured collision signal. By using Eq. (1) and the definition for δn we obtain

$$\frac{d}{dt}\delta n(t) = 2kn_A(t)n_B(t) - \delta n(t) \times \{\Gamma_{\delta n} + 2k[n_A(t) + n_B(t)]\} + k[\delta n(t)]^2, \quad (2)$$

where we use $\lambda_{A+B} = \lambda_A + \lambda_B$ and introduce the rate with which colliding molecules are lost in the *A + B* scenario via $\Gamma_{\delta n}\delta n = \Gamma_A n_A + \Gamma_B n_B - \Gamma_{A+B} n_{A+B}$. The loss rates, $\Gamma_A, \Gamma_B, \Gamma_{A+B}$, and $\Gamma_{\delta n}$ are directly obtained from the measured data (see Supplemental Material [56]). With k now being the only free parameter, we fit the solution of Eq. (2) to the measured collision signal for $\Delta t = 1$ s. The result is displayed in Fig. 3(b) for $E_c = 2.37$ kV/cm and $E_{\text{conn}} = 20$ kV/cm (high input flux), yielding $k \simeq 2 \times 10^{-8}$ cm³/s. To test whether k is a molecule-specific parameter that is independent of the density of trapped molecules, we perform a series of experiments with different control

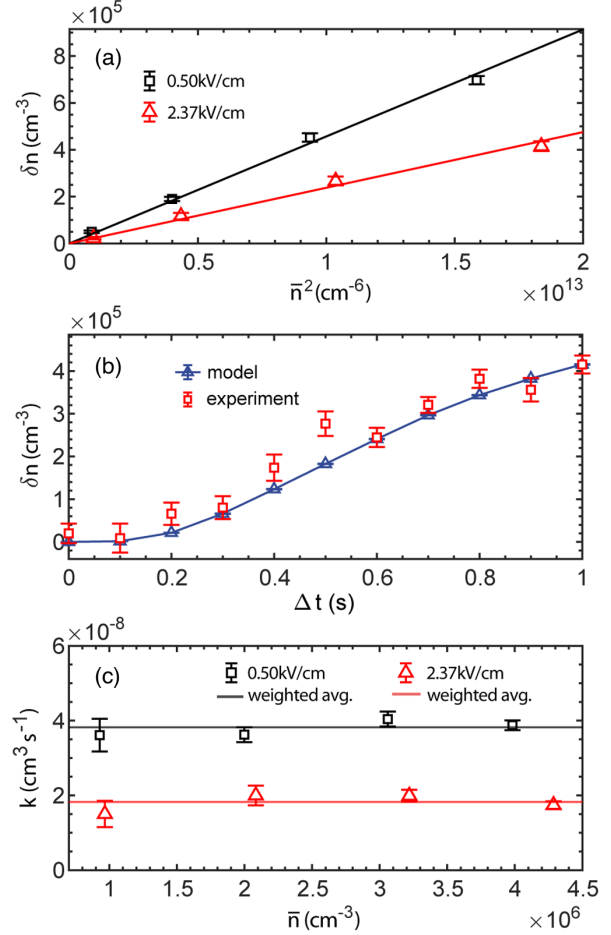


FIG. 3. Collision data. (a) Collision signal δn due to *A-B* molecules interacting for $\Delta t = 1$ s as a function of \bar{n}^2 , the product of $n_A(t)$ and $n_B(t)$ averaged over the interaction period, for two control fields. (b) Solution of Eq. (2) (blue triangles) fitted to the measured collision signal (red squares) at $\Delta t = 1$ s for $E_{\text{conn}} = 20$ kV/cm and $E_c = 2.37$ kV/cm. (c) Two-body loss-rate coefficient k plotted against \bar{n} , for two control fields. The solid lines depict the average of the measured data weighted by the respective error bars. Small changes in k ($\leq 5\%$) might occur, as tuning the loading rate slightly alters the velocity distribution of the trapped ensembles.

fields and molecule loading rates into the trap. Results are shown in Fig. 3(c) for $E_c = 0.50$ kV/cm and $E_c = 2.37$ kV/cm. For both electric fields, we observe a density independence for k , as expected for a molecule-specific parameter, but a clear electric-field dependence.

To investigate the latter in more detail, we tune the homogeneous control field E_c to six different values between 0.50 and 2.37 kV/cm and extract the corresponding values for k . The result is plotted in Fig. 4. Most striking is that k reduces by more than a factor of 2 when E_c increases from 0.50 to 2.37 kV/cm. We interpret this observation as a clear signature of dipolar relaxation: The control field induces a Stark splitting and thereby an energy mismatch between the molecular internal-angular-momentum states that are coupled

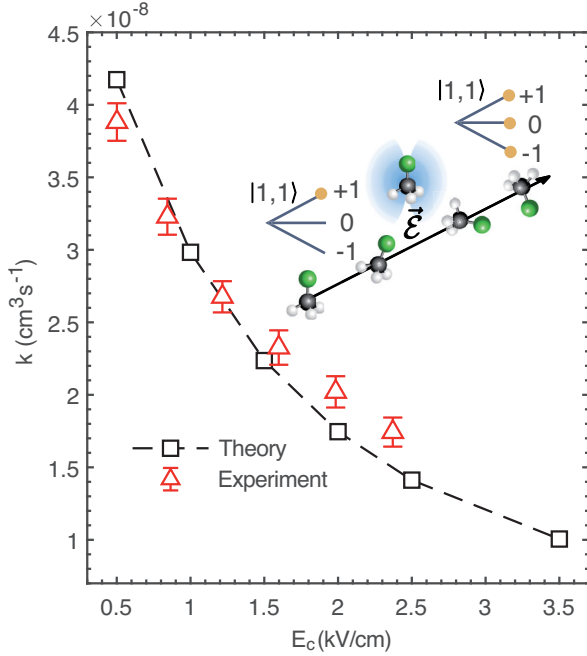


FIG. 4. Dipolar relaxation. Measured (red triangles) and calculated (black squares) two-body loss-rate coefficient k of trapped molecules versus applied control field. The dashed line is a guide to the eye. The inset shows a schematic illustration of the collision process, with molecules being redistributed to lower M states. Information on the error budget of k can be found in the Supplemental Material [56].

by the electric dipole-dipole interaction. During a nonadiabatic collision, the orientation of the dipole can change and population can be transferred from a trappable to a nontrappable state. The crucial point is that increasing the energy difference between the trappable and the nontrappable states reduces the probability for a nonadiabatic transfer. This simple picture predicts a decreasing loss-rate coefficient k for increasing control field E_c , as observed in the experiment. An electric field has already been used to control chemical reactions [6] and evaporative cooling [40] of alkali molecules, two applications distinct from our experiment. We note that for polyatomic molecules the electric field is a promising control parameter which should affect only the inelastic collisions, at least in our parameter regime. This should allow one to tune the ratio between elastic and inelastic collisions, a prerequisite for rethermalization and evaporative-cooling experiments [40,42,64].

Beyond the qualitative picture outlined above, we now compare the data in Fig. 4 with a quantitative *ab initio* model. Toward this end, we consider elastic k_{el} and inelastic k_{in} contributions to k . Note that an elastic collision between two molecules leads to loss if the kinetic energy of one molecule after the collision is larger than the trap depth. The corresponding loss-rate coefficient is obtained from $k_{\text{el}} = \sigma_{\text{loss}}^{\text{el}} v_{\text{rel}}$ for a given relative velocity v_{rel} with $\sigma_{\text{loss}}^{\text{el}}$ being the velocity-dependent elastic-loss cross section. The

latter is obtained from the differential elastic-collision cross section $(d\sigma/d\Omega)(v_{\text{rel}}, \theta)$ which is calculated using the semiclassical eikonal approximation [33]. The likelihood for a molecule to be lost from the trap after the collision, $P_{\text{loss}}(\theta, v_{\text{rel}})$ [49], is numerically determined from Monte Carlo simulations that include the electric-field distribution and the velocity distribution of the molecules in the trap. When calculating $P_{\text{loss}}(\theta, v_{\text{rel}})$, we furthermore take into account that elastic collisions change the velocity distribution and thus the single-body loss rate Γ . By averaging k_{el} over the relative-velocity distribution of the trapped molecules, we obtain $k_{\text{el}} = 4.5 \times 10^{-11} \text{ cm}^3/\text{s}$ for $E_c = 2.37 \text{ kV/cm}$, which is about three orders of magnitude smaller than two-body loss-rate coefficients reported in Fig. 4. We emphasize that, although an elastic-collision process is unlikely to lead to loss, the elastic cross section is estimated to be as large as $\sigma_{\text{el}} = 7.5 \times 10^{-12} \text{ cm}^2$.

To calculate the total inelastic-loss-rate coefficient k_{in} , we first consider loss processes described by the short-range Langevin capture model [65]. For a dipole moment of $d_{\text{avg}} = 0.83 \text{ D}$, corresponding to the average for the measured state distribution in the trap, and a control field of $E_c = 2.37 \text{ kV/cm}$, the Langevin loss-rate coefficient is obtained as $k_L = 6.8 \times 10^{-10} \text{ cm}^3/\text{s}$. This is larger than the above calculated k_{el} , but is again much smaller than the observed values displayed in Fig. 4, and is independent of E_c . Therefore, the Langevin model also fails to explain the observed losses.

To understand these, we now calculate the two-body dipolar-relaxation loss-rate coefficient k_{dd} . We do this by numerically solving the Schrödinger equation for a pair of molecules that move past each other along a fixed, straight trajectory in an electric field (see Supplemental Material [56]), as schematically illustrated in the inset of Fig. 4. The initial state vector, $|\Psi(t = -\infty)\rangle$, takes into account the rotational-state distribution in the trap in the symmetric top basis $|J, \mp K, \pm M\rangle$, with $\mp K$ chosen positive. Specifically, the molecules are statistically distributed over trappable states according to the buffer-gas cell temperature and the Stark shift. We measure the trapped state population via microwave depletion [66,67] to be $(84.8 \pm 0.7)\%$ in $|1, 1, 1\rangle$, $(7.3 \pm 0.7)\%$ in $|2, 1, 2\rangle$, and $(2.4 \pm 0.2)\%$ in $|2, 1, 1\rangle$, graphically illustrated in Fig. 1(b). The missing $(6.1 \pm 0.1)\%$ are distributed over higher-lying rotational levels with no single $|J, K, M\rangle$ state containing more than 1% of the population. The dipole-dipole interaction redistributes the initial population over trappable and nontrappable states, and the state distribution after the collision process is obtained from $|\Psi(t = +\infty)\rangle$. Summing the molecule population in nontrappable states over all possible trajectories and over the full solid angle then gives us the loss cross section $\sigma_{\text{loss}}^{dd}(v_{\text{rel}}, E_c)$ for a given relative velocity of the colliding molecules and a given control field. We do not include the full electric-field distribution as this would only slightly alter $\sigma_{\text{loss}}^{dd}$ (by $\sim 10\%$), but would increase the already

long calculation time (~ 7 months for the entire parameter space) more than tenfold. The loss-rate coefficient due to dipolar relaxation is now obtained from $k_{dd}(v_{\text{rel}}, E_c) = \sigma_{\text{loss}}^{dd}(v_{\text{rel}}, E_c)v_{\text{rel}}$, which we weight according to the measured relative-velocity distribution in the trap to get $k_{dd}(E_c)$.

The sum of the elastic and inelastic contributions to k are plotted and compared with experimental data in Fig. 4 as a function of E_c . We use the calculated values for k as an independent calibration of the molecule density, which we compare with the error-prone [49] density value derived from the QMS signal. Thereby we find a scaling factor which we globally apply for all measurements presented here. Although this factor might affect the experimental value of k , the functional dependence $k(E_c)$ as a molecule property is unaffected. We therefore attribute the observed losses to primarily (95%) dipolar relaxation. This is confirmed by the fact that k_{dd} is the only contribution with a pronounced electric-field dependence.

To conclude, we combined efficient cooling and deceleration with trapping of cold CH_3F molecules within an electric trap. We studied collisions in a clean and precisely controlled way, and changed the dipolar-relaxation loss rate by tuning the electric field. In the future we could add optoelectric Sisyphus cooling which has been applied in the same kind of trap to CH_3F [66] and H_2CO [20] for which temperatures as low as $420 \mu\text{K}$ have been reached. Collision experiments with such cold molecules would benefit from a larger elastic cross section and a smaller dipolar-relaxation loss rate, and thus could open up a route to quantum degeneracy.

This work was supported by Deutsche Forschungsgemeinschaft under Germany's excellence strategy via Munich Center for Quantum Science and Technology EXC-2111-390814868. J.P. acknowledges funding from the International Max Planck Research School for Quantum Science and Technology (IMPRS-QST) and a stipend from the Development and Promotion of Science and Technology Talents (DPST) jointly administered by the Ministry of Science and Technology, the Ministry of Education, and the Institute for the Promotion of Teaching Science and Technology (IPST) of Thailand. M.Z. acknowledges support from the Deutsche Forschungsgemeinschaft via Grant No. ZE 1096/2-1.

[1] L. D. Carr, D. DeMille, R. V. Krems, and J. Ye, *New J. Phys.* **11**, 055049 (2009).
 [2] D. Herschbach, *Faraday Discuss.* **142**, 9 (2009).
 [3] K.-K. Ni, S. Ospelkaus, D. Wang, G. Quémener, B. Neyenhuis, M. H. G. de Miranda, J. L. Bohn, J. Ye, and D. S. Jin, *Nature (London)* **464**, 1324 (2010).
 [4] G. Quémener and P. S. Julienne, *Chem. Rev.* **112**, 4949 (2012).
 [5] Y. Liu and K.-K. Ni, *Annu. Rev. Phys. Chem.* **73**, 73 (2022).

[6] W. G. Tobias, K. Matsuda, J.-R. Li, C. Miller, A. N. Carroll, T. Bilitewski, A. M. Rey, and J. Ye, *Science* **375**, 1299 (2022).
 [7] L. Santos, G. V. Shlyapnikov, P. Zoller, and M. Lewenstein, *Phys. Rev. Lett.* **85**, 1791 (2000).
 [8] M. A. Baranov, M. Dalmonte, G. Pupillo, and P. Zoller, *Chem. Rev.* **112**, 5012 (2012).
 [9] M. Wall, K. Maeda, and L. D. Carr, *New J. Phys.* **17**, 025001 (2015).
 [10] N. Y. Yao, M. P. Zaletel, D. M. Stamper-Kurn, and A. Vishwanath, *Nat. Phys.* **14**, 405 (2018).
 [11] J. A. Blackmore, L. Caldwell, P. D. Gregory, E. M. Bridge, R. Sawant, J. Aldegunde, J. Mur-Petit, D. Jaksch, J. M. Hutson, B. E. Sauer, M. R. Tarbutt, and S. L. Cornish, *Quantum Sci. Technol.* **4**, 014010 (2019).
 [12] D. DeMille, *Phys. Rev. Lett.* **88**, 067901 (2002).
 [13] S. F. Yelin, K. Kirby, and R. Côté, *Phys. Rev. A* **74**, 050301 (R) (2006).
 [14] Q. Wei, S. Kais, B. Friedrich, and D. Herschbach, *J. Chem. Phys.* **135**, 154102 (2011).
 [15] K.-K. Ni, T. Rosenband, and D. D. Grimes, *Chem. Sci.* **9**, 6830 (2018).
 [16] P. Yu, L. W. Cheuk, I. Kozyryev, and J. M. Doyle, *New J. Phys.* **21**, 093049 (2019).
 [17] P. D. Gregory, J. A. Blackmore, S. L. Bromley, J. M. Hutson, and S. L. Cornish, *Nat. Phys.* **17**, 1149 (2021).
 [18] M. Zeppenfeld, M. Motsch, P. W. H. Pinkse, and G. Rempe, *Phys. Rev. A* **80**, 041401(R) (2009).
 [19] C. H. Townes and A. L. Schawlow, *Microwave Spectroscopy* (Dover Publications, Inc., New York, 1975).
 [20] A. Prehn, M. Ibrügger, R. Glöckner, G. Rempe, and M. Zeppenfeld, *Phys. Rev. Lett.* **116**, 063005 (2016).
 [21] J. D. Weinstein, R. DeCarvalho, T. Guillet, B. Friedrich, and J. M. Doyle, *Nature (London)* **395**, 148 (1998).
 [22] H. L. Bethlem, G. Berden, F. M. H. Crompvoets, R. T. Jongma, A. J. A. van Rooij, and G. Meijer, *Nature (London)* **406**, 491 (2000).
 [23] S. Y. T. van de Meerakker, P. H. M. Smeets, N. Vanhaecke, R. T. Jongma, and G. Meijer, *Phys. Rev. Lett.* **94**, 023004 (2005).
 [24] T. Rieger, T. Junglen, S. A. Rangwala, P. W. H. Pinkse, and G. Rempe, *Phys. Rev. Lett.* **95**, 173002 (2005).
 [25] B. C. Sawyer, B. L. Lev, E. R. Hudson, B. K. Stuhl, M. Lara, J. L. Bohn, and J. Ye, *Phys. Rev. Lett.* **98**, 253002 (2007).
 [26] B. G. U. Englert, M. Mielenz, C. Sommer, J. Bayerl, M. Motsch, P. W. H. Pinkse, G. Rempe, and M. Zeppenfeld, *Phys. Rev. Lett.* **107**, 263003 (2011).
 [27] N. Akerman, M. Karpov, Y. Segev, N. Bibelnik, J. Narevicius, and E. Narevicius, *Phys. Rev. Lett.* **119**, 073204 (2017).
 [28] D. J. McCarron, M. H. Steinecker, Y. Zhu, and D. DeMille, *Phys. Rev. Lett.* **121**, 013202 (2018).
 [29] H. J. Williams, L. Caldwell, N. J. Fitch, S. Truppe, J. Rodewald, E. A. Hinds, B. E. Sauer, and M. R. Tarbutt, *Phys. Rev. Lett.* **120**, 163201 (2018).
 [30] S. E. Maxwell, N. Brahm, R. deCarvalho, D. R. Glenn, J. S. Helton, S. Nguyen, D. Patterson, J. Petricka, D. DeMille, and J. M. Doyle, *Phys. Rev. Lett.* **95**, 173201 (2005).
 [31] R. Glöckner, A. Prehn, B. G. U. Englert, G. Rempe, and M. Zeppenfeld, *Phys. Rev. Lett.* **115**, 233001 (2015).

- [32] X. Wu, T. Gantner, M. Zeppenfeld, S. Chervenkov, and G. Rempe, *ChemPhysChem* **17**, 3631 (2016).
- [33] J. L. Bohn, M. Cavagnero, and C. Ticknor, *New J. Phys.* **11**, 055039 (2009).
- [34] A. V. Gorshkov, P. Rabl, G. Pupillo, A. Micheli, P. Zoller, M. D. Lukin, and H. P. Büchler, *Phys. Rev. Lett.* **101**, 073201 (2008).
- [35] G. Quéméner and J. L. Bohn, *Phys. Rev. A* **83**, 012705 (2011).
- [36] T. Karman and J. M. Hutson, *Phys. Rev. Lett.* **121**, 163401 (2018).
- [37] T. Xie, M. Lepers, R. Vexiau, A. Orbán, O. Dulieu, and N. Bouloufa-Maafa, *Phys. Rev. Lett.* **125**, 153202 (2020).
- [38] S. Ospelkaus, K.-K. Ni, D. Wang, M. H. G. de Miranda, B. Neyenhuis, G. Quéméner, P. S. Julienne, J. L. Bohn, D. S. Jin, and J. Ye, *Science* **327**, 853 (2010).
- [39] Z. Z. Yan, J. W. Park, Y. Ni, H. Loh, S. Will, T. Karman, and M. Zwierlein, *Phys. Rev. Lett.* **125**, 063401 (2020).
- [40] J.-R. Li, W. G. Tobias, K. Matsuda, C. Miller, G. Valtolina, L. De Marco, R. R. W. Wang, L. Lassablière, G. Quéméner, J. L. Bohn, and J. Ye, *Nat. Phys.* **17**, 1144 (2021).
- [41] M.-G. Hu, Y. Liu, M. A. Nichols, L. Zhu, G. Quéméner, O. Dulieu, and K.-K. Ni, *Nat. Chem.* **13**, 435 (2021).
- [42] A. Schindewolf, R. Bause, X.-Y. Chen, M. Duda, T. Karman, I. Bloch, and X.-Y. Luo, [arXiv:2201.05143](https://arxiv.org/abs/2201.05143).
- [43] M. Guo, X. Ye, J. He, M. L. González-Martínez, R. Vexiau, G. Quéméner, and D. Wang, *Phys. Rev. X* **8**, 041044 (2018).
- [44] P. D. Gregory, M. D. Frye, J. A. Blackmore, E. M. Bridge, R. Sawant, J. M. Hutson, and S. L. Cornish, *Nat. Commun.* **10**, 3104 (2019).
- [45] Y. Segev, M. Pitzer, M. Karpov, N. Akerman, J. Narevicius, and E. Narevicius, *Nature (London)* **572**, 189 (2019).
- [46] L. W. Cheuk, L. Anderegg, Y. Bao, S. Burchesky, S. S. Yu, W. Ketterle, K.-K. Ni, and J. M. Doyle, *Phys. Rev. Lett.* **125**, 043401 (2020).
- [47] L. Anderegg, S. Burchesky, Y. Bao, S. S. Yu, T. Karman, E. Chae, K.-K. Ni, W. Ketterle, and J. M. Doyle, *Science* **373**, 779 (2021).
- [48] B. C. Sawyer, B. K. Stuhl, M. Yeo, T. V. Tscherbul, M. T. Hummon, Y. Xia, J. Klos, D. Patterson, J. M. Doyle, and J. Ye, *Phys. Chem. Chem. Phys.* **13**, 19059 (2011).
- [49] X. Wu, T. Gantner, M. Koller, M. Zeppenfeld, S. Chervenkov, and G. Rempe, *Science* **358**, 645 (2017).
- [50] A. P. P. van der Poel, P. C. Zieger, S. Y. T. van de Meerakker, J. Loreau, A. van der Avoird, and H. L. Bethlem, *Phys. Rev. Lett.* **120**, 033402 (2018).
- [51] N. B. Vilas, C. Hallas, L. Anderegg, P. Robichaud, A. Winnicki, D. Mitra, and J. M. Doyle, [arXiv:2112.08349](https://arxiv.org/abs/2112.08349).
- [52] J. L. Bohn, *Phys. Rev. A* **63**, 052714 (2001).
- [53] N. R. Hutzler, H.-I. Lu, and J. M. Doyle, *Chem. Rev.* **112**, 4803 (2012).
- [54] S. Chervenkov, X. Wu, J. Bayerl, A. Rohlfes, T. Gantner, M. Zeppenfeld, and G. Rempe, *Phys. Rev. Lett.* **112**, 013001 (2014).
- [55] C. Sommer, M. Motsch, S. Chervenkov, L. D. van Buuren, M. Zeppenfeld, P. W. H. Pinkse, and G. Rempe, *Phys. Rev. A* **82**, 013410 (2010).
- [56] See Supplemental Material at <http://link.aps.org/supplemental/10.1103/PhysRevLett.128.203401> for additional information on experimental details and the calculation of the two-body loss-rate coefficient, which includes Refs. [57–61].
- [57] B. G. U. Englert, Ph.D. thesis, Technische Universität München, 2013.
- [58] M. L. Wall, K. Maeda, and L. D. Carr, *Ann. Phys. (Berlin)* **525**, 845 (2013).
- [59] A. R. Edmonds, *Angular Momentum in Quantum Mechanics* (Princeton University Press, Princeton, 1996).
- [60] M. Zeppenfeld, *Europhys. Lett.* **118**, 13002 (2017).
- [61] D. Zhang and S. Willitsch, *Cold Chemistry: Molecular Scattering and Reactivity Near Absolute Zero* (RSC Publishing, 2017).
- [62] M. Kirste, B. G. Sartakov, M. Schnell, and G. Meijer, *Phys. Rev. A* **79**, 051401(R) (2009).
- [63] M. Zeppenfeld, Ph.D. thesis, Technische Universität München, 2013.
- [64] H. Son, J. J. Park, W. Ketterle, and A. O. Jamison, *Nature (London)* **580**, 197 (2020).
- [65] M. T. Bell and T. P. Softley, *Mol. Phys.* **107**, 99 (2009).
- [66] M. Zeppenfeld, B. G. U. Englert, R. Glöckner, A. Prehn, M. Mielenz, C. Sommer, L. D. van Buuren, M. Motsch, and G. Rempe, *Nature (London)* **491**, 570 (2012).
- [67] R. Glöckner, A. Prehn, G. Rempe, and M. Zeppenfeld, *New J. Phys.* **17**, 055022 (2015).